A neutron diffraction investigation into the rhombohedral phases of the perovskite series $PbZr_{1-x}Ti_xO_3$

1998 J. Phys.: Condens. Matter 10 6251

(http://iopscience.iop.org/0953-8984/10/28/007)

J. Phys.: Condens. Matter **10** (1998) 6251–6269. Printed in the UK PII: S0953-8984(98)93322-7

A neutron diffraction investigation into the rhombohedral phases of the perovskite series $PbZr_{1-x}Ti_xO_3$

D L Corker†‖, A M Glazer†, R W Whatmore‡, A Stallard‡ and F Fauth§

† Department of Physics, Clarendon Laboratory, Parks Road, The University of Oxford, Oxford OX1 3PU, UK

‡ School of Industrial and Manufacturing Science, Cranfield University, Cranfield, Bedfordshire MK43 0AL, UK

§ Institut Laue–Langevin, BP 156, F-38042, Grenoble Cédex 9, France

Received 16 April 1998

Abstract. Rietveld refinements using neutron powder profiles are reported for a series of $PbZr_{1-x}Ti_xO_3$ samples (commonly known as PZT), with x ranging from ≈0.12 to ≈0.40. Cation shifts, octahedral distortion and tilts are determined with varying composition across the ferroelectric rhombohedral regions, $F_{R(LT)}$ and $F_{R(HT)}$, of the PZT phase diagram. These parameters are then used in conjunction with a simple Landau–Devonshire model to investigate the nature of the $F_{R(LT)}$–$F_{R(HT)}$ phase transition.

It is found that the cation shifts, octahedral distortion and tilt angles decrease with increasing Ti content, but, surprisingly, the octahedral strain, as indicated by the rhombohedral angle, increases. This is in contrast to the case for all other known rhombohedral perovskites. Furthermore, the refined anisotropic displacement parameters of the cations are anomalous and cannot be accounted for by the average crystal structure. A model is presented in which a domain-type 'local' structure is considered, containing 'ordered' additional cation displacements, consistently with the reports of extra reflections observed in electron microscopy studies by Viehland *et al*, Dai *et al* and Ricote *et al*.

1. Introduction

The solid solution series $PbZr_{1-x}Ti_xO_3$ (PZT) displays a rich and complex phase diagram, as shown in figure 1. Although at high temperatures these compounds exhibit a high-symmetry, primitive cubic structure, at lower temperatures a variety of cation shifts, octahedral tilts and deformations occur leading to a number of different structures. At room temperature these include the lower-symmetry, antiferroelectric, orthorhombic, A_O, structure of $PbZrO_3$ (Corker *et al* 1997). With increasing Ti content, two ferroelectric, rhombohedral phases, $F_{R(LT)}$ and $F_{R(HT)}$, are observed up to around $x \approx 0.50$ where there is a transition to a ferroelectric tetragonal phase, F_T, continuing through to the end member $PbTiO_3$ (Glazer and Mabud 1978). The boundary between the $F_{R(HT)}$ and F_T phases is known as the *morphotropic phase boundary*, and has been the subject of intense scientific scrutiny. In this report, Rietveld refinements of neutron powder diffraction profiles are used to investigate the rhombohedral $F_{R(LT)}$ region and the $F_{R(LT)}$–$F_{R(HT)}$ interface observed at room temperature.

Both the rhombohedral and the tetragonal ferroelectric regions of PZT have been of considerable technological importance for many years. The interest in the rhombohedral

‖ Present address: School of Industrial and Manufacturing Science, Cranfield University, Cranfield, Bedfordshire MK43 0AL, UK; e-mail: corker@physics.ox.ac.uk.

0953-8984/98/286251+19$19.50

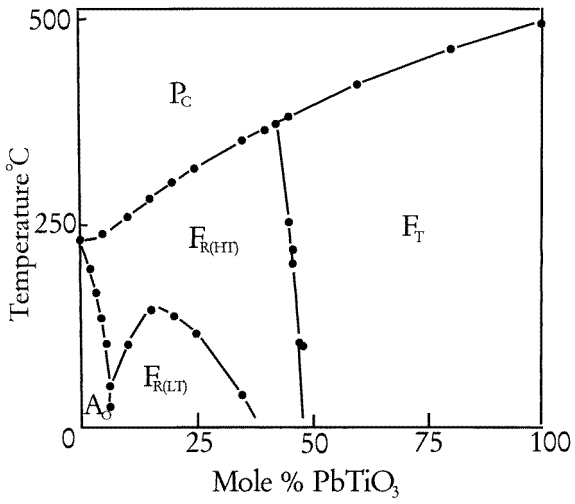

Figure 1. The phase diagram of the PZT solid solution series (from Jaffe *et al* 1971).

region originates mainly from its application in uncooled thermal detectors. At room temperature the rhombohedral $F_{R(LT)}$ phase has space group $R3c$ and exhibits both cation shifts along $[111]_p$ and octahedra tilted about $[111]_p$†. As temperature increases the octahedral tilts are known to disappear (Glazer and Mabud 1978), leading to the phase transition to $F_{R(HT)}$, and space group $R3m$. In this phase, the cations remain shifted in parallel fashion along $[111]_p$. A further increase in temperature diminishes the cation shifts until the final phase transition into the cubic perovskite structure occurs. It is this sequence of loss of spontaneous polarization with increasing temperature which gives PZT its large pyroelectric coefficient, dP_s/dt, and hence its value in uncooled thermal IR detection applications.

Temperature dependence studies of the cation shifts and octahedral tilts have been reported on for $x \approx 0.35$ and $x \approx 0.10$ by Cereceda *et al* (1997) and Glazer *et al* (1978a) respectively. This same $F_{R(LT)}$–$F_{R(HT)}$ phase transition sequence is not only observed with increasing temperature, but also when the amount of Ti in the PZT is increased. However, despite the industrial importance of this ferroelectric region, no systematic investigation of these structural features with varying composition has previously been undertaken. This new study reports on seven samples prepared to span the entire $F_{R(LT)}$ region, such that structural trends with composition in this region can be derived.

2. Structural parameters

At room temperature the $F_{R(LT)}$ phase has octahedra tilted about $[111]_p$. In the notation of Glazer (1972, 1975), this is represented by the tilt system $a^-a^-a^-$ and results in cell doubling of all three pseudo-cubic axes, hence forming a unit cell containing eight formula units. Parallel displacements of the cations are also known to exist along $[111]_p$. The

† The subscript 'p' refers to a choice of axes corresponding to the pseudo-cubic cell of the perovskite structure.

transition $F_{R(LT)}$–$F_{R(HT)}$ described to date can therefore be summarized as below:

$F_{R(LT)}$ phase	$\Rightarrow$	$F_{R(HT)}$ phase
Tilt system $a^-a^-a^-$	Increasing temperature	Tilt system $a^0a^0a^0$
Space group $R3c$	or	Space group $R3m$
Unit cell $(2a_p \times 2a_p \times 2a_p)$	Increasing Ti content	Unit cell $(a_p \times a_p \times a_p)$
Cation shifts $[111]_p$	$\Rightarrow$	Cation shifts$[111]_p$

In this report the structure will be referred to hexagonal axes, whose lattice parameters a_H and c_H, are related to the pseudo-cubic cell $(2a_p \times 2b_p \times 2c_p)$ by the transformation

$$\begin{pmatrix} 0.5 & 0 & -0.5 \\ -0.5 & 0.5 & 0 \\ 1 & 1 & \end{pmatrix}.$$

This setting allows the important structural characteristics, described by refinable parameters, denoted s, t, d and e, to be extracted easily from any refined atomic coordinates. This procedure was originally developed for rhombohedral perovskites in general by Megaw and Darlington (1975) and leads to the set of atomic fractional coordinates shown in table 1.

Table 1. Fractional coordinates for the hexagonal setting of rhombohedral perovskites, space group $R3c$ (for space group $R3m$, the parameter e is equal to zero), in terms of independent refinable parameters developed by Megaw and Darlington (1975).

Atom type	x/a	y/b	z/c
Pb	0.00	0.00	$s + 0.25$
Ti/Zr	0.00	0.00	t
O	$1/6 - 2e - 2d$	$1/3 - 4d$	$1/12$

The independent parameters have the following meanings:

s: fractional shift of Pb along c_H (or $[111]_p$)

t: fractional shift of Zr/Ti along c_H (or $[111]_p$)

d: describes a distortion of the oxygen octahedron, keeping triad-axis symmetry, but making upper and lower faces (with respect to c_H) different in size

e: parameter relating to tilt of octahedron about c_H (or $[111]_p$). The angle of tilt ω is given by the formula $\tan\omega = 4\sqrt{3}e$

As the cell doubling originates from the $a^-a^-a^-$ tilt system, the true hexagonal cell should halve its volume (as c_H is reduced by a factor of 2), on going from $F_{R(LT)}$ to $F_{R(HT)}$. However, for consistency, although the parameter e theoretically vanishes in the final sample, which is in the $F_{R(HT)}$ phase at room temperature, it is convenient to continue the Rietveld refinement in the large unit cell and space group $R3c$. This is allowed by restricting any O(y) shift, calculated by the Rietveld procedure, to being double the corresponding O(x) shift, allowing the parameter d to refine and yet restricting e to being equal to zero.

3. Material preparation

In order to achieve a homogeneous Zr/Ti ratio in each of the polycrystalline PZT samples used for the powder neutron diffraction, the conventional ceramic technique of firing mixed

oxides was discarded in favour of the recently established alkoxide route. In this technique, the appropriate proportions of Zr and Ti alkoxides were first weighed under nitrogen and then refluxed for one hour with dry isopropyl alcohol (IPA). After the specimens had been allowed to cool, excess water was slowly added while the solution was continuously stirred. The mixture was then decanted and allowed to dry to form a fine-grained, homogeneous powder. The resultant amorphous sample was then fired at 973 K for four hours. This produced a $ZrTiO_4$ phase in which the Zr and Ti were mixed on an interatomic scale. At this stage, Pb was added by milling the powder with PbO in IPA. After drying, 5 wt% polyvinyl acetate (PVA) binder was added and pellets 20 mm in diameter were pressed. After biscuiting at 773 K, the pellets were sintered at 1523 K for six hours, ground and then sieved. Powder x-ray diffraction measured using a STOE Stadi-P x-ray diffractometer showed the expected powder patterns with only a small amount of impurity in the first sample, PZT08, identified as pyrochlore. Henceforth, to denote the samples made, we shall adopt the notation PZTxx, where xx is the *nominal* percentage Ti content.

4. Neutron data collection

Accurate structural determinations of these materials have in the past been inhibited by the difficulty of preparing single-domain crystals. It was therefore decided that neutron polycrystalline diffraction was not only the best method to use to prevent erroneous data arising from unobserved twins, but also that it would allow reasonable precision to be achieved in the determination of the oxygen fractional coordinates, which is often problematic with conventional x-ray analysis.

Table 2. Experimental details of the neutron diffraction data collections and refinements.

Data collection details		Refinement and analysis details	
Radiation	Neutrons	Background	Linear interpolation
Wavelength (Å)	1.9114	Weighting scheme	$(\sigma^2)^{-1}$
Absorption correction	None	$(\Delta/\sigma)_{max}$	0.1
Diffractometer type	D1A, ILL	Refinement	FULLPROF (Rodriguez-Carvajal 1995)
Monochromator	Germanium		
2θ-step (deg)	0.05	Full width at half-maximum	$U\tan^2\theta + V\tan\theta + W$
Crystal system	Rhombohedral	No of parameters used	52
Space group	$R3c$	Analytic function for profile	Pseudo-Voigt
Temperature (K)	293	Graphics	Crystallographica (Oxford Cryosystems 1996)
Sample containers	Vanadium holder		
Instrument geometry	25 ^{3}He detectors		
θ_{max} (deg)	79.475		

Neutron powder data were collected at room temperature using the diffractometer D1A at the Institut Max Von Laue–Paul Langevin (Grenoble, France). The PZT polycrystalline samples were held in cylindrical vanadium holders of diameter 1 cm and height 6 cm. Neutron data were collected over the range $3.75^\circ < 2\theta < 157.45^\circ$, in 0.05° steps, and with $\lambda = 1.9114$ Å. The program FULLPROF (Rodriguez-Carvajal 1995) was used for the Rietveld refinement with neutron scattering factors $b_{Pb} = 9.405$ fm, $b_{Zr} = 7.160$ fm, $b_{Ti} = -0.3438$ fm and $b_O = 5.803$ fm. The background was corrected by means of a linear interpolation between given points, taken from each profile, while the peak shapes were described by pseudo-Voigt profiles. Table 2 lists the experimental details.

The initial atomic coordinates for the first sample, PZT08, were taken from the

Table 3. Parameters obtained from Rietveld refinement. Note that the strain parameter ζ and the angle $(90-\alpha)$ are calculated from the unit-cell parameters, and the tilt angle ω is calculated from the parameter e.

	PZT08	PZT13	PZT18	PZT23	PZT28	PZT33	PZT38
a_H (Å)	5.8461(1)	5.83670(9)	5.82376(8)	5.8134(1)	5.8010(1)	5.7851(1)	5.7692(1)
c_H (Å)	14.4182(3)	14.3989(2)	14.3716(2)	14.3500(3)	14.3230(3)	14.2880(3)	14.2501(2)
Ti (%)	12.9(3)	16.2(3)	20.4(3)	25.5(3)	30.0(3)	34.8(3)	39.9(3)
s	0.0331(2)	0.0330(1)	0.0323(1)	0.0321(2)	0.0315(1)	0.0217(4)	0.0174(4)
t_{Zr}	0.0125(5)	0.0141(2)	0.0142(2)	0.0132(3)	0.0123(7)	0.0021(6)	−0.0030(8)
t_{Ti}	0.012(7)	0.026(2)	0.025(1)	0.021(2)	0.016(3)	0.0359(8)	0.0360(9)
$-d$	0.00353(6)	0.00326(5)	0.00312(5)	0.00300(6)	0.00271(6)	0.00237(7)	0.00194(8)
e	0.0145(1)	0.0133(1)	0.0116(1)	0.0099(1)	0.0078(1)	0.0041(1)	0.0000(1)
ω (deg)	5.75(4)	5.27(4)	4.61(4)	3.94(4)	3.08(4)	1.61(4)	0.01(4)
$\zeta \times 10^2$	0.18	0.28	0.42	0.53	0.68	0.78	0.84
$90-\alpha$ (deg)	0.262	0.272	0.284	0.295	0.311	0.316	0.320
Pb U^{11} (Å^2)	0.0190(2)	0.0194(2)	0.0202(2)	0.0217(2)	0.0234(2)	0.0227(2)	0.0219(3)
Pb U^{33} (Å^2)	0.0014(1)	0.0015(1)	0.0014(1)	0.0012(1)	0.0014(1)	−0.0005(1)	−0.0007(1)
Zr/Ti U_{iso} (Å^2)	0.0004(4)	0.0007(3)	0.0006(4)	0.0007(3)	0.0011(5)	0.0004(2)	0.0038(2)
O U^{11} (Å^2)	0.0184(4)	0.0179(4)	0.0186(4)	0.0203(6)	0.0221(9)	0.0191(9)	0.017(1)
O U^{22} (Å^2)	0.0072(4)	0.0064(4)	0.0081(3)	0.0083(4)	0.0088(5)	0.0151(5)	0.0151(6)
O U^{33} (Å^2)	0.0027(1)	0.0022(1)	0.0022(1)	0.0028(1)	0.0028(1)	0.0130(2)	0.0138(2)
O U^{12} (Å^2)	0.001(1)	0.000(1)	0.0023(9)	0.003(1)	0.003(1)	0.004(2)	0.003(2)
O U^{13} (Å^2)	−0.0003(5)	−0.0007(5)	−0.0015(5)	−0.0011(8)	−0.0022(7)	−0.0019(7)	−0.001(2)
O U^{23} (Å^2)	−0.0024(2)	−0.0018(2)	−0.0020(2)	−0.0018(2)	−0.0017(3)	−0.0085(4)	−0.009(5)
R_p (%)	3.62	3.31	2.93	3.06	3.36	3.64	3.84
R_w (%)	5.05	4.51	3.99	4.42	4.83	5.20	5.59

determination for PZT ($x \approx 0.10$) by Glazer *et al* (1978a). Models for subsequent samples containing successively greater levels of Ti were each taken from the previous refinement. Apart from that for the final sample, PZT38, all of the refinements converged quickly. For PZT38, the preliminary refinement in the space group $R3c$ was made to converge with difficulty, although it was soon apparent that $e = 0$ within errors, signifying the phase transition from $F_{R(LT)}$–$F_{R(HT)}$ and the associated reduction in cell size. However, as described previously, for consistency the cell was not reduced, but instead a false mirror plane was inserted by imposing the restriction $\Delta O(y) = 2\,\Delta O(x)$. With this constraint the refinement continued without further problems. In addition, refinement of the Zr/Ti site as a single atom tended to give negative displacement parameters, and as a result we allowed the Zr and Ti sites to be refined independently, but with equivalent isotropic displacement parameters. The refined structural parameters are given in table 3. It should be noted that refinement of the site occupation gave compositions slightly higher than the nominal compositions, suggesting that more Ti has entered the unit cells than expected.

As reported in the previous Rietveld analysis of PZT with $x = 10$ (Glazer *et al* 1978a), isotropic refinements of this phase yielded poor profile fits. Therefore, although refinements of anisotropic displacement parameters (U^{ij}) from conventional neutron diffraction profiles have to be approached with caution, investigation revealed that a far better agreement

between calculated and experimental profiles was achieved when they were allowed to refine.

It can be seen that the anisotropic displacement parameters for the oxygen are physically reasonable across the series and very consistent from sample to sample. However, the Pb and Zr/Ti (when originally refined as a single entity) displacement parameters show highly anisotropic components that are physically unreasonable, although they are consistent across the series, and with others reported for this phase by Glazer *et al* (1978a).

In all cases the Pb displacement parameters describe a disc-shaped ellipsoid severely flattened along the (threefold) c_{H}-axis (i.e. in the direction of the cation shifts themselves) and yet extended perpendicular to this direction. With the degree of elongation perpendicular to this axis, it is no surprise that the inclusion of these parameters into the refinement has a large effect not only on the profile fit, but also on the refined Pb positional parameters. This peculiar feature is not limited purely to neutron experiments, but was also recognized as early as 1953 (Sawaguchi 1953), on the basis of the observation of the intensities of x-ray powder diffraction lines. We obtained further support for the existence of this feature when the sample PZT23 was examined by means of conventional x-ray diffraction. Data were collected over the 2θ-range 10°–100°, with a step size of 0.01°, at room temperature using a Siemens D5005 x-ray diffractometer. Although the data collected were insufficiently numerous for an accurate, full-structural Rietveld analysis, the package Win-Rietveld was used in combination with a model based on the structure derived from the neutron study for the refinement of the Pb site. Again, a considerably improved profile fit was achieved when anisotropic displacements were refined. Assuming a Pearson VII profile and a simple linear interpolation as a background correction, the refinement soon converged, giving the profile parameters $R_p = 14.36\%$, $R_{wp} = 21.69\%$, $a_{\mathrm{H}} = 5.8138(8)$ Å and $c_{\mathrm{H}} = 14.3523(4)$ Å. The atomic parameters for Pb refined to the values Pb(z) = 0.284(1), Pb(U^{11}) = 0.010(1) Å^2 and Pb(U^{33}) = 0.0001(1) Å^2, again consistent with the disc-shaped anisotropic displacement ellipsoid derived from the neutron study.

With both x-ray and neutron investigations, in this and previously reported studies, indicating physically unreasonable anisotropic displacement parameters, we therefore must assume that the anomaly is caused by an inherent PZT structural characteristic. This is clearly an important feature; further analysis of these anisotropic displacement parameters is presented later in relation to a possible disorder of the cations.

5. Analysis of the average structure

The physically unreasonable anisotropic displacement parameters are an indication that the average structure, given by either x-ray or neutron diffraction analysis, does not represent the true structure of this region of the PZT phase diagram. Nevertheless, examination of the atomic parameters established by this method is important for many reasons. Firstly, to date there have been many reports where correlating perovskite structural features, such as octahedral tilts and distortion, has been attempted. Unfortunately, for structural details any previous analysis has had to rely on data scattered throughout the literature on very different perovskites and where structure determinations have been achieved through varying techniques. Hence, any investigation such as this, wherein the entire procedure from material preparation to analysis technique is kept constant throughout, yields valuable consistent data for future parameter–parameter correlation or parameter–property correlation theoretical examinations.

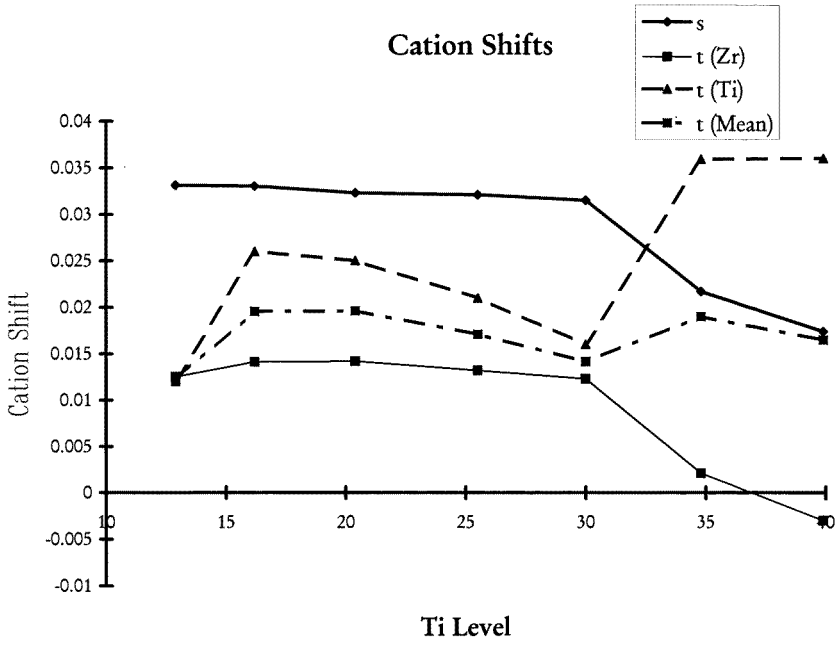

Figure 2. Variations of the cation shifts (expressed in fractions of c_H) with the percentage of Ti.

5.1. Cation shifts

As discussed earlier, the parameters t and s describe the displacement of the Zr/Ti from the octahedron centre and the Pb atoms from the cubic twelvefold-coordinated site observed in an ideal cubic perovskite structure. Figure 2 shows the Pb, Zr and Ti refined shifts plotted as functions of Ti content. The Pb shifts and the weighted average of the Zr/Ti shifts found in the Rietveld refinement are roughly constant as the Ti content increases, or possibly show a gradual decrease. If we consider the Zr and Ti shifts independently, despite the roughness of the results (especially for Ti, principally because there is less Ti than Zr), an interesting trend can be seen. The Zr shifts are approximately the same as the Ti shifts for the lowest Ti concentration, but then the two shifts diverge, especially above 30% Ti, with the Ti shift increasing and the Zr shift decreasing to zero. We believe that this indicates that as the Ti content increases, the large difference in ionic radius and polarizability between Zr and Ti becomes more effective in differentiating between unit cells containing Zr and those containing Ti. In support of this, it is generally found in perovskites that Zr tends to occupy the centres of octahedra (e.g. in $BaZrO_3$, $PbZrO_3$, $SrZrO_3$), whereas the more highly polarizable and smaller Ti moves off-centre (e.g. in $BaTiO_3$, $PbTiO_3$).

5.2. The octahedral tilt angle, ω

Figure 3 shows the variation in the experimentally determined tilt angle with the composition, showing clearly that it decreases with increasing Ti content, until the $F_{R(LT)}$–$F_{R(HT)}$ boundary is reached.

Discussions of the octahedral tilt angle as an order parameter in the expansion for the free energy have been reported many times (see, e.g., Cereceda *et al* 1997) in association with the PZT rhombohedral $F_{R(LT)}$–$F_{R(HT)}$ phase transition. All of the investigations have

been limited to this transition observed as the temperature changes and usually restricted to a single PZT composition. There are only two exceptions, Benguigui (1972) and Pinczuk (1973), where attempts have been made to use the Landau theory of the perovskite ferroelectric to explain PZT phase transitions observed with compositional variation. As in both these cases the investigations were used in order to describe the morphotropic phase boundary ($F_{R(HT)}$–F_T), the possibility of treating the octahedral tilt angle 'ω' as an order parameter was never approached.

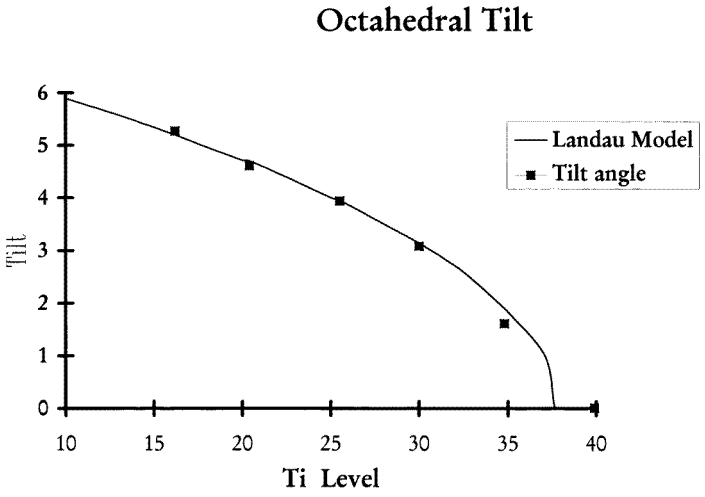

Figure 3. The variation of the octahedron tilt angle ω with the percentage of Ti. The continuous line was calculated according to a simple Landau model (see the text).

If in the Landau theory we replace the temperature by the composition, x = % of Ti, we would expect the tilt angle to depend on x, thus:

$$\omega^2 = a(x_0 - x)/x_0$$

where a is a constant and x_0 is the composition at which the tilt angle vanishes, i.e. at which the $F_{R(LT)}$–$F_{R(HT)}$ transition occurs.

Least-squares refinement of this expression using the *refine* program in the Crystallographica software (Oxford Cryosystems 1996) gave a good fit with $x_0 = 37.9\%$. The tilt angles calculated using this relation, along with experimentally determined values, are shown in figure 3.

5.3. The octahedral distortion, d

The octahedral distortion remains negative across the series, which means that the upper face of the octahedron is bigger than the lower. This is consistent with the fact that the Zr/Ti displacements are directed towards the upper face. The variation of the octahedral distortion with Ti is shown in figure 4. Like the tilt angle, this too decreases linearly with the percentage of Ti, although it does not go to zero when $\omega = 0$; this is to be expected since the $F_{R(HT)}$ phase is still rhombohedral.

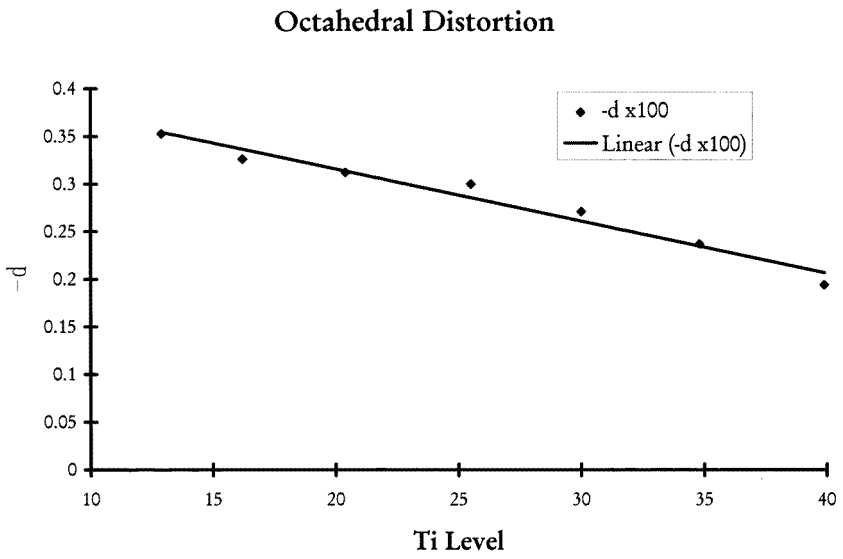

Figure 4. The variation of the magnitude of the octahedral distortion d with the percentage of Ti.

5.4. The octahedral strain, ζ

In addition to the tilt angle, we should consider including the octahedral strain in the calculations, as was done earlier by Clarke and Glazer (1976) in describing the behaviour of the $PbZr_{1-x}Ti_xO_3$, $x = 10$, $F_{R(LT)}$–$F_{R(HT)}$ transition observed with varying temperature. The octahedral strain was defined by Megaw and Darlington (1975), where the factor $1+\zeta$ is the elongation or compression of the octahedron along c_H. This quantity is not refined from the structural coordinates, but can only be calculated from the unit-cell dimensions, and so must not be confused with the parameters s, t, d or e. In terms of the hexagonal unit-cell parameters,

$$\zeta = \cos\omega\left(\frac{c_H}{a_H\sqrt{6}}\right) - 1$$

With respect to the pseudo-cubic cell, the strain is related to the departure of the rhombohedral angle α_p from 90° by the formula

$$\cos\alpha_p = \frac{c_H^2 - 6a_H^2}{c_H^2 + 12a_H^2}.$$

It has been considered that there should be some connection between the octahedral strain and the angle of tilt in perovskites, and a rough relationship of this type was found by Megaw and Darlington (1975) in an examination of all of the perovskites known of at that time. Indeed, one would expect from simple geometrical considerations that the magnitude of the strain, and hence $|90 - \alpha_p|$, should increase with increase of the tilt angle, as was found by Megaw and Darlington.

Figure 5 shows the experimentally determined octahedral strain plotted against the composition. The remarkable and unexpected thing to note is that, in this case, despite the decrease in the tilt angle ω, with increasing Ti, the strain of the octahedra, ζ, increases towards the $F_{R(LT)}$–$F_{R(HT)}$ transition boundary! This behaviour appears to be at odds

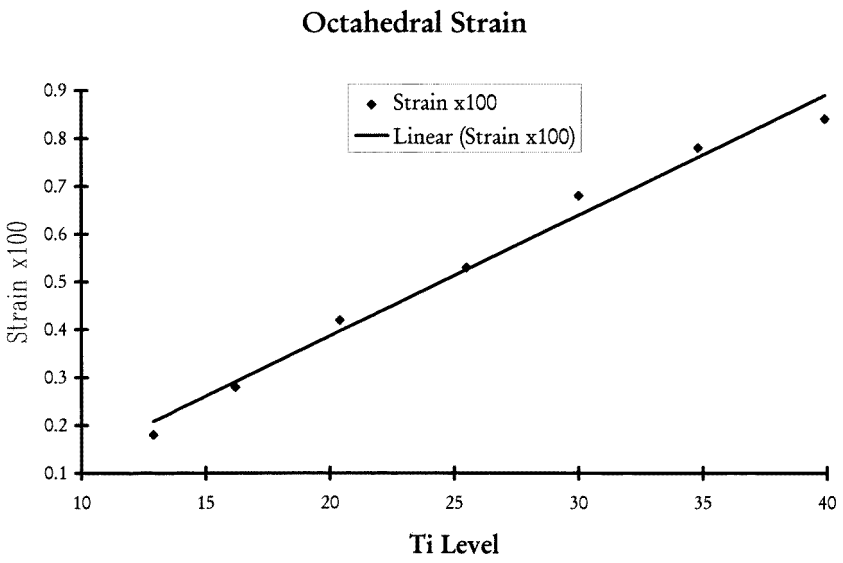

Figure 5. The variation of the octahedral strain ζ with the percentage of Ti.

with that for all other known perovskites, and cannot be explained by the conventional geometrical picture of the perovskite structure. This is observed when both of the transitions are approached by either increasing the Ti content or by increasing the temperature. We propose an explanation for this phenomenon later.

From close observation, it is found that the strain obeys a linear relationship with the Ti content, except perhaps in the $F_{R(HT)}$ region at high Ti content. A good least-squares linear fit is obtained (figure 5):

$$\zeta = 0.0251 \times \text{percentage of Ti} - 0.105.$$

When extrapolated backwards, this relation predicts that the strain vanishes when the Ti level is reduced to approximately 6%. From previous experimental investigations, and as shown in figure 1, this is where the $F_{R(LT)}$–A_o transition takes place, indicating a possible link between the octahedral strain and the orthorhombic–rhombohedral transition.

5.5. The nature of the phase transition

Although the features described so far seem to indicate that the transition observed with composition variation and that observed with increase in temperature are very similar, there are some important differences in the behaviour of these parameters which have not been addressed so far. For instance, consider the values given by Clarke and Glazer (1976) for the $F_{R(LT)}$–$F_{R(HT)}$ transition with temperature observed in $PbZr_{1-x}Ti_xO_3$, $x = 0.1$. In this instance the octahedral tilt decreases as the transition is approached from below. However, at the transition the tilt becomes zero 'discontinuously', indicating a first-order transition. Clearly, this is in contrast to the smooth extrapolation to zero observed for the tilt as the Ti level increases in figure 3, indicating a more second-order behaviour. The change in strain through this transition is much more abrupt when the transition is observed in $PbZr_{1-x}Ti_xO_3$, $x = 0.1$, with temperature variation than when observed with composition variation. It is therefore instructive to rewrite the expansion of the Gibbs energy function in terms of both

ω and ζ as previously given by Clarke and Glazer:

$$G = G_0 + \tfrac{1}{2}a\omega^2 + \tfrac{1}{4}b\omega^4 + \tfrac{1}{6}c\omega^6 + d\zeta + \tfrac{1}{2}e\zeta^2 + f\omega^2\zeta. \quad (1)$$

Minimizing with respect to ζ gives the relation

$$\zeta = -d/e - (f/e)\omega^2. \quad (2)$$

The first point to notice is that including the third-order coupling between the tilt order parameter ω and the octahedral strain predicts a linear variation of ζ with composition as shown in figure 5. Secondly, if equation (2) is inserted back into equation (1), the coupling coefficient f becomes an important feature, describing whether the transition is of first or second order:

$$G = G_0 + \tfrac{1}{2}a\omega^2 + (\tfrac{1}{4}b - f^2/e)\omega^4 + \cdots.$$

When f is large, the coefficient of ω^4 becomes negative and a first-order transition is observed, as in $PbZr_{1-x}Ti_xO_3$, $x = 0.1$. However, when the coupling between these two parameters is relatively small, a more second-order transition, as regards composition, is expected.

With this description we can hence relate the discontinuous and continuous behaviour of the tilt and strain parameters observed with temperature and composition variation, respectively, to the degree of coupling between them. Further examination of this feature and a possible suggestion for the change in coupling is presented later in association with achieving fourfold Pb–O bonding.

6. The local structure

From the above, there are two issues of serious concern that need explanation.

(1) The Pb anisotropic displacement ellipsoids consistently refine as flat discs lying perpendicular to the c_H-axis (i.e. perpendicular to the $[111]_p$ cation shift direction). This general disc shape does not vary significantly with composition. The Zr/Ti displacement parameters are also abnormally small.

(2) The octahedral strain increases as the tilt angle decreases with Ti content, in contradiction to the behaviour found for all other known perovskites.

Neither of these observations can be explained in terms of the *average* crystal structure that is obtained by x-ray or neutron refinement. We believe that it is necessary to consider a certain amount of disorder of the cation positions in order to reconcile these observations. Support for this notion comes from recent electron microscopy studies of this PZT region (Viehland *et al* 1993, Dai *et al* 1995) where extra reflections of the type $\{\frac{1}{2}, \frac{1}{2}, 0_p\}$ and $\{\frac{1}{2}, \frac{1}{2}, \frac{1}{2}_p\}$ are observable at low Ti levels in the rhombohedral phases. Such reflections should be systematically absent according to the $R3c$ symmetry. In order to explain the appearance of these reflections in electron diffraction investigations, which were not observable in x-ray and neutron diffraction investigations, the extra reflections were associated by the above authors with short-range ordering of different octahedral tilt systems.

However, in a more recent study by Ricote *et al* (1997), electron diffraction simulations led to the conclusion that the effect could not be due to octahedral tilts. Ricote *et al* (1997) suggested instead that there is short-range order involving cation shifts in some way different from those of the simple c_H ($[111]_p$) type. In particular, domains with cation shifts of the type $[1\bar{1}0]_p$ were proposed. Effectively superimposing 'nanoscale' domains with

$[\bar{1}10]_p$, $[10\bar{1}]_p$, $[01\bar{1}]_p$ cation shifts gives rise to the average $[111]_p$ shifts observed in this study. If such cation shifts were for the most part completely disordered, both neutron and x-ray diffraction studies would lead to 'average' $[111]_p$ cation shifts, and so it would not be surprising to find that refinement of the respective anisotropic displacement parameters would appear to give physically unreasonable shapes.

In order to investigate this possibility, the data were refined allowing the Pb atoms to occupy positions away from the threefold axis, with each component atom having one-third occupancy. The space group was kept as $R3c$, but no symmetry restrictions were placed on the x- and y-coordinates of the Pb atoms. Although a very crude approach, with Pb(x), Pb(y) and Pb(z) now refining independently, this allows the Pb to shift not only along the c_H-axis (i.e. $[111]_p$) but also in any direction perpendicular to this direction. The introduction of three sites is also consistent with a model similar in nature to that proposed by Ricote *et al* (1997), as for every domain with a $[110]_p$ displacement, there will on average always be a corresponding domain with a $[101]_p$ shift etc.

This technique was applied to PZT08. The refinement quickly converged to Pb(x) = 0.015(3), Pb(y) = 0.040(2) and Pb(z) = 0.2826(2). Although the errors in these positions are quite large, when the model was systematically altered for different starting positions, to avoid local minima, the final converged values were always consistent. It is also worth noting that the simultaneous refinement of the anisotropic displacement parameters refined to Pb(U^{11}) = 0.003(1) Å^2 and Pb(U^{33}) = 0.006(1) Å^2, showing a clear reduction of the ellipsoid elongation perpendicular to the threefold axis. Applying this procedure to the other compositions in all but the final case, where no convergence could be reached, gave similar values.

Table 4. Refined atomic coordinates of the Pb disorder sites in both hexagonal and pseudo-cubic cells. The two other symmetry-related sites in the pseudo-cubic cell are determined by simple permutation of the coordinates.

Sample	x_H	y_H	z_H	x_{pc}	y_{pc}	z_{pc}
PZT08	0.015	0.040	0.283	0.275	0.270	0.303
PZT13	0.012	0.042	0.283	0.276	0.267	0.303
PZT18	0.011	0.040	0.282	0.277	0.268	0.302
PZT23	0.016	0.047	0.282	0.274	0.267	0.306
PZT28	0.016	0.042	0.281	0.273	0.268	0.302
PZT33	0.017	0.038	0.276	0.268	0.266	0.295

In order to discover the meaning of the above Pb positions, we now transform the coordinates to the pseudo-cubic frame of reference. With the refined Pb atomic coordinates of PZT08, three positions are generated surrounding the original Pb site shifted along $[111]_p$ only:

$$(0.015, 0.040, 0.283)$$
$$(-0.040, -0.025, 0.283)$$
$$(0.025, -0.015, 0.830).$$

There are consistent with the symmetry operators (x, y, z), $(-y, x-y, z)$ and $(y-x, -x, z)$†.

† Three further sites would also be generated through the translation of $z + 1/2$.

On using the transformation matrix

$$\begin{pmatrix} \frac{1}{2} & 0 & -\frac{1}{2} \\ -\frac{1}{2} & \frac{1}{2} & 0 \\ 1 & 1 & 1 \end{pmatrix}$$

the associated coordinates in the large pseudo-cubic cell translate as approximately:

(0.275, 0.270, 0.303)

(0.303, 0.273, 0.270)

(0.270, 0.303, 0.273).

The completely unshifted Pb site, i.e. that in the ideal perovskite cubic structure, would lie at (0.25, 0.25, 0.25). Therefore, within the errors of the refinement, the refined coordinates from the hexagonal cell represent a common $[111]_p$ shift as expected, in combination with $[100]_p$, $[010]_p$ or $[001]_p$ shifts. The refined $[111]_p$ shift is slightly smaller than that predicted in the usual refinement procedure, while the $[100]_p$-type shifts are of approximately 0.2 Å. Refined atomic coordinates for samples PZT08–PZT33 are given in table 4, along with coordinates translated, as described above, into the pseudo-cubic cell. The effect of averaging over the three $[100]_p$ shifts is to simulate the flat displacement ellipsoid found in the refinement of the average structure.

It may be noted that although a consistently satisfactory convergence could not be reached for PZT38, it is not proposed that the extra shifts implied by the other refinements are not also present in this sample. The anisotropic displacement parameters given by the usual Rietveld analysis are still highly anisotropic, and when the usual Pb site is replaced by three sites with extra $[100]_p$-type shifts attached and the anisotropic displacements factors refined, the associated ellipsoid again becomes more isotropic and physically reasonable.

6.1. $[100]_p$ Pb shifts

In summary, from further refinement of the Pb site using conventional neutron Rietveld refinement, it seems likely that the true Pb site is disordered over three possible sites. Each site corresponds to the expected $[111]_p$ shift of the average structure, followed by an extra $[100]_p$-type shift. Although the precise magnitudes of these extra shifts cannot be taken literally, since they were obtained by such a crude approach, the approximate value of 0.2 Å seems physically reasonable. However, for this disorder to be given further support, we must consider a physical basis for it. The answer to this problem is found when one views the structural implications of these extra shifts for the Pb–O bonding.

To illustrate this feature, we reconsider the Pb–O bonding derived from the usual refinement. Here Pb is able to from three short bonds with oxygen at 2.526 Å and a further three at 2.794 Å, where the exact values were calculated from the coordinates of PZT08. However, in both the orthorhombic and tetragonal phases of PZT it is known that Pb favours a short fourfold coordination. By re-examining the Pb coordination with the extra $[100]_p$-type displacements predicted by the above refinement, this is also what we find. Again using the values obtained for PZT08, we calculate four short Pb–O bonds of lengths 2.43, 2.51, 2.64 and 2.66 Å with the remaining two bond distances at 2.76 and 2.93 Å.

When the entire compositional range is re-examined, the same situation, where threefold coordination is replaced by fourfold, is continued through the addition of these extra shifts. When first visualized, this fourth short bond appears to be achieved through a combination of these extra shifts and also octahedral tilt. It may therefore be expected that, as Ti levels

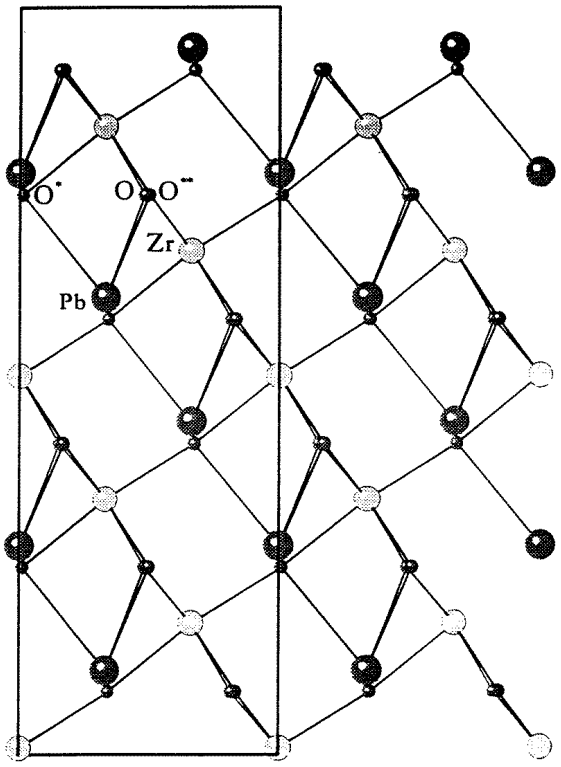

(a)

Figure 6. (a) Showing a projection on $(100)_H$ of PZT33. The three short Pb–O bonds associated with $[111]_p$ Pb displacements are depicted in relation to the ZrO_6 network. (b) Showing a projection on $(100)_H$ of PZT33, but where the single Pb site is replaced by three disordered Pb sites. For each site the associated fourfold coordination is observed.

increase and the tilt angle diminishes, the fourth extra bond would become more difficult to form. However, when the geometry of this extra bond is analysed more carefully, it is found that the negative effect of decreasing the tilt angle can be overcome by an increase in the octahedral strain, which is indeed what is observed from the experimental results.

The predicted bond distances of PZT33 at the opposite end of the PZT rhombohedral region show the success of this compensating effect. From the usual refinement, where Pb is restricted to being shifted along $[111]_p$, the three short bond distances are 2.549 Å, while three longer bonds are calculated to be at 2.872 Å. When any of the extra shifts are incorporated, four short Pb–O bonds are achieved at the lengths 2.51, 2.54, 2.71 and 2.71 Å, while the further two bonds lengths are 2.80 and 2.85 Å.

The physical reasoning behind this compensating effect can be seen by examination of figure 6(a), where the three short Pb–O bonds, represented by Pb–O, Pb–O* and Pb–O**, associated with $[111]_p$ Pb shifts only, are shown in relation to the ZrO_6 octahedral network. In figure 6(b), the usual Pb site is replaced by the three sites achievable with the extra $\langle 100\rangle_p$ shifts. As can be observed, all extra Pb–O short bonds achieved with this arrangement lie approximately in planes such as plane X and plane X^* shown in the diagram. Therefore all the fourth 'extra' bonds are almost perpendicular to the c_H-axis. Hence, as the Ti level

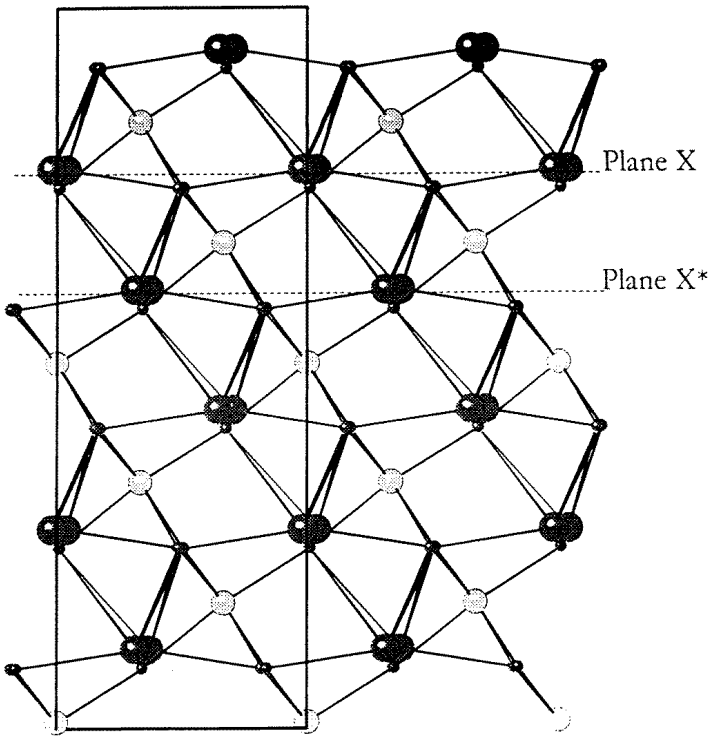

(b)

Figure 6. (Continued)

increases, if a_H decreases disproportionately faster than c_H (i.e. the strain increases), then the extra Pb–O bond is achieved more easily, while at the same time having a minimal effect on the three other bonds. We therefore find that similarly disordered cations throughout the rhombohedral PZT region acquire short, fourfold-coordinated Pb–O bonding through a combination of octahedral tilts and strain.

The combined effect of the octahedral strain and tilt in achieving this fourfold coordination also gives a physical basis for the coupling observed between these parameters as discussed earlier. Taking this argument further, we may also postulate again that the coupling observed with increasing temperature diminishes as compositions with higher Ti contents are examined. The reduction in the strength of this coupling could be explained by the reduction in unit-cell volume when the smaller Ti replaces Zr. As the cell volume decreases, it is not as important that the strain increases and the tilt decreases, as it is easier for the Pb to achieve four short Pb–O bonds in the smaller cell. The effects of cell volume will not only be a consideration in terms of the level of Ti present in the composition, but will also be a factor at high Zr levels, where a much larger thermal expansion will be apparent. From this line of thought, we therefore expect that further investigations of the $F_{R(LT)}$–$F_{R(HT)}$ transition observed with temperature variation, but on samples with greater Ti content than those that have been measured to date, would show more continuous characteristics, i.e. as the Ti level increases we would expect that the $F_{R(LT)}$–$F_{R(HT)}$ transition observed with temperature variation would transform gradually from a first-order-type to a second-order-type transition.

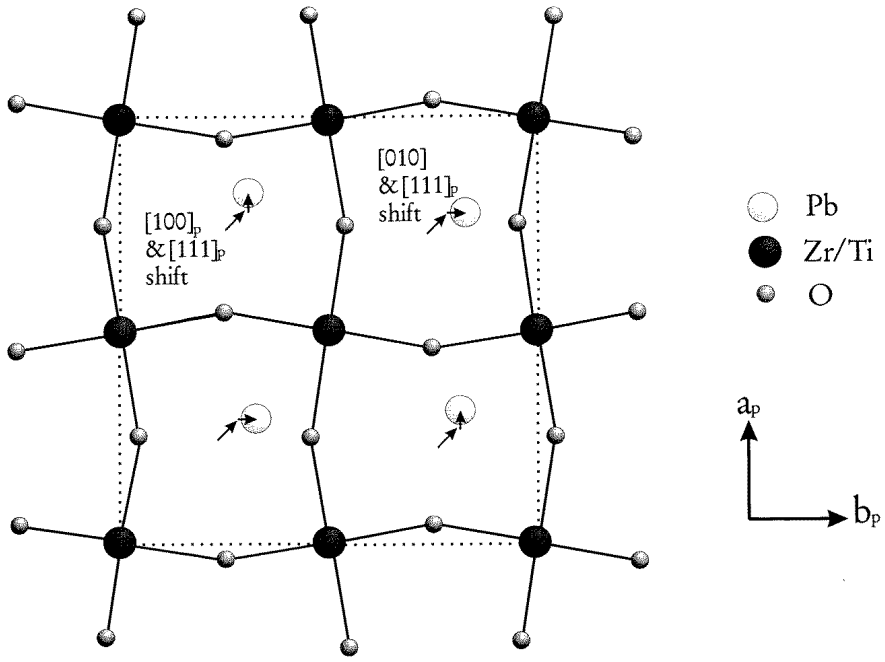

Figure 7. A structural model incorporating $[111]_p$- and $[100]_p$-type shifts capable of generating the extra reflections of the type $\{\frac{1}{2}, \frac{1}{2}, 0_p\}$ seen in electron microscopy studies.

At first sight, the reliability of predicting structural disorder from simple neutron powder diffraction has to be questioned. However, increasing octahedral strain with decreasing octahedral tilt has never before been reported, and goes against long-established perovskite characteristics. The disordered model proposed here goes a long way towards explaining this phenomenon. A potentially important aspect of this model is that the $\langle 100 \rangle_p$ shifts act as a precursor to the tetragonal phase on the other side of the morphotropic phase boundary, which occurs at higher Ti content. The tetragonal phase is characterized by large $[100]_p$ cation shifts.

6.2. Zr and Ti shifts

The possibility that Zr and Ti shifts diverge, as found in the first set of refinements, should not be overlooked in the context of explaining the anomalous octahedral strain behaviour. The refined Ti shift is the only internal structural coordinate that appears to increase with Ti content, and so this is the only internal parameter that increases in line with the octahedral strain. The movement of the Ti towards one of the faces of the oxygen octahedron is likely, via repulsion, to cause the oxygens on that face to move further away, thus elongating the octahedron, as is found.

6.3. The relation to extra reflections observed in electron microscopy

Evidence for a structural disorder has been reported many times in connection with extra reflections observed in electron microscopy. Quite different models for this disorder have been suggested. We therefore conclude by presenting a model based on the proposed Pb

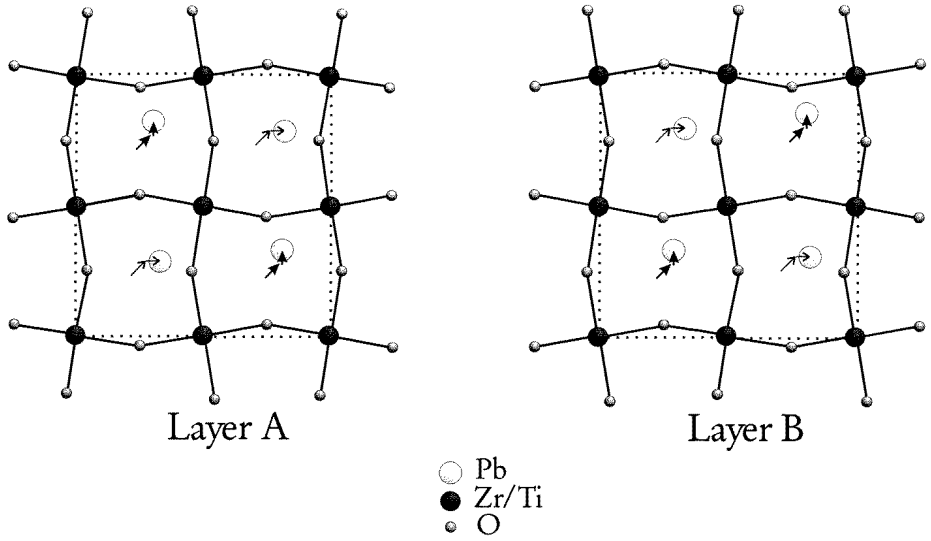

Figure 8. A structural model of dimensions $2a_p \times 2a_p \times 2a_p$, split into two layers A and B, such that the sequence of $[111]_p$- and $[100]_p$-type shifts can be visualized. This model is capable of producing the extra reflections of the type $\{\frac{1}{2}, \frac{1}{2}, \frac{1}{2}\}_p$ seen in electron microscopy studies.

disorder, which would support the observations of these extra reflections.

Energetically, under normal circumstances in the bulk structure, there is no reason to suggest that any of the 'extra' $[100]_p$-type shifts should be more favourable than the others. Therefore, if we consider that the extra $[100]_p$-type shifts, superimposed on $[111]_p$ shifts, are perfectly random throughout the entire structure we would expect no extra reflections to be observed in any type of diffraction analysis. However, different types of diffraction technique see different amounts of the sample. In electron microscopy the surface structure is dominant in any diffraction image observed. Under these circumstances, where perhaps 'uniaxial' stresses are commonplace, it would not be inconceivable for two of the three types of shift, say $[100]_p$ and $[010]_p$, to become energetically preferable. We would expect to find 'short-range' order in local domains generated on the surface. For example, two types of possible local structure are shown in figure 7 and figure 8, for the $2a_p \times 2a_p \times a_p$ and the $2a_p \times 2a_p \times 2a_p$ pseudo-cubic cells respectively. Certainly the magnitude of the $[100]_p$ shifts predicted by the above refinements of $\sim$0.2 Å, when ordered in a manner such as is shown in the figures, would generate the extra reflections reported by previous authors at approximately the correct intensities.

The disappearance of extra reflections observed in electron microscopy studies as Ti levels increase could in many respects be linked to the appearance of the morphotropic phase boundary. As this boundary is approached, all of the PZT phases have increasingly similar free energies. Energetically, cation shifts along any of the directions $\langle 100\rangle_p$, $\langle 110\rangle_p$ or $\langle 111\rangle_p$ become equivalent and hence complicated domains become apparent. Similarly, it is therefore reasonable that, although at low Ti levels certain configurations of extra cation $[100]_p$ shifts may become preferable to total disorder, this energy difference is again likely to decrease as Ti levels increase and the morphotropic phase boundary is approached. As it is this preferred configuration which induces 'short-range' order, the appearance of these extra reflections would hence decrease as Ti levels increase.

7. Summary

In conclusion, an examination of several compositions throughout the rhombohedral PZT region using conventional neutron powder diffraction has given much valuable information. General trends of cation displacements and the various deviations of the octahedral network from the ideal cubic perovskite model have been established. Basic Landau theory has also been successfully applied to the $F_{R(LT)}$–$F_{R(HT)}$ transition observed with composition variation rather than temperature variation for the first time. Simple least-squares fitting of the observed parameters shows a good fit of the predicted relationship between the tilt order parameter 'ω' and the octahedral strain.

Through the refinement of three disordered Pb sites, it has also been predicted that throughout the rhombohedral PZT region, random $\langle 100 \rangle_p$ shifts are superimposed on the established $[111]_p$ Pb shifts. These extra shifts generate fourfold coordination for the Pb cation and also a physical basis for the observed coupling between the octahedral strain and tilt.

It has long been understood (Pinczuk 1973) that short-range interactions between neighbouring ions become much stronger with decreasing Ti. Consequently, far from the morphotropic phase boundary, short-range ordering of $[100]_p$ shifts results in extra reflections. The size and position of these domains limit the observation of extra reflections to electron diffraction only. Likely factors contributing to domain creation are surface stress, 'usual' domain wall stress, impurities, or even thermal stress caused by the electron microscopy itself. This final option would also support the observation of extra reflections at low Ti levels, as the comparatively high thermal expansion coefficient of the sample would magnify any respective stress caused by a thermal gradient.

For the bulk material, however, it is proposed that the effect of these extra disordered cation shifts is not completely undetectable through conventional x-ray and neutron diffraction. Refinement of cation anisotropic displacement ellipsoids leads to physically unreasonable flattening in the $[111]_p$ direction and elongation perpendicular to this direction, as the ellipsoid 'attempts' to emulate the three possible sites at which the Pb can 'sit'. If these unreasonable displacement parameters are allowed to remain in the refinement, reasonable profile fits can be achieved and hence this anomaly has so far been overlooked. However, as demonstrated above, further refinement where Pb shifts perpendicular to the $[111]_p$ direction are allowed yields sites consistent with random $\sim$0.2 Å shifts along $\langle 100 \rangle_p$ directions.

Acknowledgments

The authors would like to thank the Institut Max von Laue–Paul Langevin (ILL), Grenoble, France, for allowing the neutron diffraction experiment to be carried out. We would also like to thank Peter Cross for his assistance during our time at the ILL. We would also like to express gratitude to the Engineering and Physical Sciences Research Council (EPSRC) for providing the grant for this investigation.

References

Benguigui 1972 *Solid State Commun.* **11** 825–8

Cereceda N, Noheda B, Iglesias T, Fernandez-del-Castillo J R, Gonzalo J A, Duan N, Wang Y L, Cox D E and Shirane G 1997 *Phys. Rev.* B **55** 6174–9

Clarke R and Glazer A M 1976 *Ferroelectrics* **12** 207–9

Corker D L, Glazer A M, Dec J, Roleder K and Whatmore R 1997 *Acta Crystallogr.* B **53** 135–42

Dai X, Zu Z and Viehland D 1995 *J. Am. Ceram. Soc*. **76** 2815–27
Glazer A M 1972 *Acta Crystallogr.* B **28** 3384–92
——1975 *Acta Crystallogr*. A **31** 756–62
Glazer A M and Mabud S A 1978 *Acta Crystallogr*. B **34** 1065–70
Glazer A M, Mabud S A and Clarke R 1978a *Acta. Crystallogr*. B **34** 1060–5
——1978b *Acta Crystallogr*. B **34** 1065–70
Jaffe B, Cook W R and Jaffe H 1971 *Piezoelectric Ceramics* (London: Academic)
Megaw H D and Darlington C N W 1975 *Acta Crystallogr.* A **31** 161–73
Oxford Cryosystems 1996 *Crystallographica. A Crystallographic Data Software Tool* Oxford Cryosystems, Long Hanborough, UK
Pinczuk A 1973 *Solid State Commun.* **12** 1035–8
Ricote J, Corker D L, Whatmore R W, Impey S A, Glazer A M, Dec J and Roleder K 1998 *J. Phys.: Condens. Matter* **10** 1767–86
Rodriguez-Carvajal J 1995 *FULLPROF. A Rietveld Refinement and Pattern Matching Analysis Program* Laboratoire Leon Brillouin (CEA-CNRS), France
Sawaguchi E 1953 *J. Phys. Soc. Japan* **8** 615–29
Viehland D, Xu Z and Payne D A 1993 *J. Appl. Phys.* **74** 7454–60